Ab Initio Study of the Hydrogen Exchange Reaction at Group 3 and 4 Metals in Comparison to That at Alkali Metals

Arndt H. Neuhaus, Eric D. Glendening, and Andrew Streitwieser*

Department of Chemistry, University of California at Berkeley, Berkeley, California 94720-1460

Received May 10, 1996[⊗]

Computations are reported at several theoretical levels for the exchange reaction of group 3 and 4 metal hydrides with hydrogen. At the CISD+Q level weak complexes are formed with an association energy of 0.1−3.0 kcal mol^{-1}. The transition states for the exchange with group 3 transition metals have C_{2v} symmetry and an energy of 8−10 kcal mol^{-1} relative to the reactants. This barrier is lower than that for exchange of alkali-metal hydrides with hydrogen (15.7−21.7 kcal mol^{-1}) and much lower than for exchange of group 4 transition-metal hydrides (31.5−45.9 kcal mol^{-1}). The transition states of alkali-metal hydrides approximate ion pairs of the alkali-metal cations with H_3^- ion, whereas the transition-metal cases involve bonding interactions with empty d orbitals.

Introduction

Experimental studies of the Bercaw group[1,2] have shown that bis(pentamethylcyclopentadienyl)scandium hydride undergoes facile hydrogen exchange with dihydrogen. Similar exchange reactions occur with alkanes. Comparable reactions have been demonstrated for some lanthanides[3] and actinides.[4−7] An important question concerns the nature of the transition states of these exchange reactions. Bonds to early transition elements and to lanthanides are known to have high ionic character, but these elements also have d orbitals that may be involved in bonding. An appropriate comparison would be with the alkali-metal systems, but a proper experimental comparison is difficult. The scandium, lanthanide, and actinide studies made use of pentamethylcyclopentadienyl derivatives in solution. This approach cannot be applied to the monovalent alkali metals, whose hydrides are highly aggregated, nonvolatile, and insoluble. Theory, however, is not limited by such experimental limitations, and we report such a comparison of group 3 and 4 transition metals with alkali-metal analogs in this paper.

We replace the pentamethylcyclopentadienyl groups by hydrogen for computational feasibility and compare the exchange reactions of group 3 and 4 transition-metal hydrides, MH_3 and MH_4, respectively, with hydrogen with the related reactions of lithium, sodium, and potassium hydride. The latter reactions have already been studied computationally by Schleyer and Kaufman,[8] Ziegler,[9] and Rappé and Upton.[10] To their work we add additional configuration interaction studies and analyses of the electronic structures of the transition states. Relatively few theoretical studies at sufficiently high level have been reported for organometallic compounds or reactions of group 3 metals, even though they are closed-shell systems that should have fewer computational problems than other transition-metal compounds. Available studies include the $Sc(C_2H_4)^+$ cation[11] and reactions of the Sc−H bond with acetylene[12] and carbon monoxide,[13] as well as some hydrogen activation reactions.[14]

Methods

Ab initio wave functions were calculated by GAMESS[15] using the standard double-ζ basis sets listed in Table 1. The hydrogen basis was augmented with an s-type diffuse function and a set of p-type polarization functions to describe the anionic character of this atom when bound to a metal center. Effective core potentials (ECP) for the transition metals are those of Hay and Wadt.[16,17] Molecular geometries were optimized within the designated symmetry constraints for self-consistent field (SCF)[18] and complete active space SCF (CASSCF)[19−27] wave functions. Due to the shallow nature of

[⊗] Abstract published in *Advance ACS Abstracts,* August 1, 1996.

(1) Bercaw, J. E. *Pure Appl. Chem.* **1990**, *62*, 1151−1154.
(2) Piers, W. E.; Shapiro, P. J.; Bunel, E. E.; Bercaw, J. E. *Synlett* **1990**, 74−84.
(3) Watson, P. L.; Parshall, G. W. *Acc. Chem. Res.* **1985**, *18*, 51−56.
(4) Bruno, J. W.; Marks, T. J.; Day, V. W. *J. Am. Chem. Soc.* **1982**, *104*, 7357−7360.
(5) Bruno, J. W.; Smith, G. M.; Marks, T. J.; Fair, C. K.; Schultz, A. J.; Williams, J. M. *J. Am. Chem. Soc.* **1986**, *108*, 40−56.
(6) Fendrick, C. M.; Marks, T. J. *J. Am. Chem. Soc.* **1986**, *108*, 425−437.
(7) Fagan, P. J.; Manriquez, J. M.; Maatta, E. A.; Seyam, A. M.; Marks, T. J. *J. Am. Chem. Soc.* **1981**, *103*, 6650−6667.
(8) Kaufmann, E.; Schleyer, P. v. R. *J. Comput. Chem.* **1989**, *10*, 437.
(9) Ziegler, T.; Folga, E.; Berces, A. *J. Am. Chem. Soc.* **1993**, *115*, 636−646.
(10) Rappe, A. K.; Upton, T. H. *J. Am. Chem. Soc.* **1992**, *114*, 7509−7517.
(11) Sarasa, J. P.; Poblet, J. M.; Anglada, J.; Caballol, R. *Chem. Phys. Lett.* **1990**, *167*, 421−428.
(12) Rappe, A. K. *Organometallics* **1990**, *9*, 466−475.
(13) Rappe, A. K. *J. Am. Chem. Soc.* **1987**, *109*, 5605−5613.
(14) Rappe, A. K.; Upton, T. H. *J. Chem. Phys.* **1986**, *85*, 4400.
(15) GAMESS: Schmidt, M. W.; Baldridge, K. K.; Boatz, J. A.; Elbert, S. T.; Gordon, M. S.; Jensen, J. H.; Koseki, S.; Matsunaga, N.; Nguyen, K. A.; Su, S.; Windus, T. L.; Dupuis, M.; Montgomery, J. A., Jr. *J. Comput. Chem.* **1993**, *14*, 1347.
(16) Hay, P. J.; Wadt, W. R. *J. Chem. Phys.* **1985**, *82*, 299−310.
(17) For an authoritative review of pseudopotentials in transition-metal compounds see: Frenking, G.; Antes, I.; Böhme, M.; Dapprich, S.; Ehlers, A. W.; Jonas, V.; Neuhaus, A.; Otto, M.; Stegmann, R.; Veldkamp, A.; Vyboishchikov, S. F. In *Reviews in Computational Chemistry*; Lipkowitz, K. B., Boyd, D. B., Eds.; VCH: New York, 1995; Vol. 7.
(18) Roothaan, C. C. J. *Rev. Mod. Phys.* **1951**, *23*, 69.
(19) Feller, D. F.; Schmidt, M. W.; Ruedenberg, K. *J. Am. Chem. Soc.* **1982**, *104*, 960−967.
(20) Yarkony, D. R. *Chem. Phys. Lett.* **1981**, *77*, 634−635.

S0276-7333(96)00350-0 CCC: $12.00

Table 1. Basis Sets Used for the Calculations

center	contraction	ref
H	(5s1p)/[3s1p][a]	42, 43
Li	(9s4p)/[4s2p]	44
Na	(12s8p1d)/[6s4p1d][b]	45
K	(14s9p1d)/[6s4p1d][c]	46
Cs	(5s5p4d)/[3s3p2d]	47
Sc (full valence)	(14s9p5d)/[8s4p2d]	46
Sc (ecp)	(5s5p5d)/[3s3p2d]	16
Y	(5s6p4d)/[3s3p2d]	16
La	(5s6p3d)/[3s3p2d]	16
Ti	(5s5p5d)/[3s3p2d]	5
Zr	(5s6p4d)/[3s3p2d]	16
Hf	(5s6p3d)/[3s3p2d]	16

[a] Includes a diffuse s-type function ($\alpha_s = 0.036$[48]) and p-type polarization ($\alpha_p = 1.0$[43]) functions. [b] Includes d-type polarization functions ($\alpha_d = 0.175$[49]). [c] Includes d-type polarization functions ($\alpha_d = 0.1$[49]).

the potential energy surface, all complex and transition state geometries were converged with a conservative gradient threshold of 0.00001 au, and each geometry was characterized by harmonic vibrational analysis.

Since single-reference methods often provide an inadequate description of metal-containing compounds, the SCF study was extended to the CASSCF level. These calculations were initially performed with an active space that contained all *n* bonding, nonbonding, and antibonding orbitals (designated CAS[*n*]). However, it became apparent during the course of this investigation (*vide infra*) that the CAS[*n*] wave functions neglect important correlation effects, and the active space was subsequently extended by one or two orbitals. Details of these wave functions are given in Table 2.

Electron correlation effects were examined with second-order Møller−Plesset (MP2)[28] and configuration interaction (CI) methods[29] with frozen core orbitals. Calculations at these levels were applied to the SCF optimized geometries. Single and double CI wave functions were calculated for each system, and where appropriate, the reported energies include Davidson's size-consistency correction.[30] Full valence CI wave functions were also calculated for the alkali-metal MH_3 systems, which have only two valence electrons.

Natural population and natural bond orbital (NPA/NBO) analysis[31−38] was performed for each wave function except MP2. This method uses an occupancy-weighted symmetric orthogonalization procedure to construct a set of "natural atomic orbitals" (NAOs) from which atomic charges ("natural charges") are evaluated. One-, two-, and three-center "natural bond orbitals" (NBOs) are then calculated from local block eigenfunctions of the NAO density matrix. The set of formally occupied NBOs typically accounts for greater than 99% of the electron density, with the remainder residing in the antibonding and low-lying Rydberg orbitals. The occupancies of the latter arise from electron delocalization or charge transfer (CT) out of the occupied NBOs. The importance of this effect can be assessed by evaluating the second-order interaction (eq 1),

$$\Delta E^{(2)} = -2\frac{\langle\sigma|F|\sigma^*\rangle^2}{\Delta\epsilon} \qquad (1)$$

where $\langle\sigma|F|\sigma^*\rangle$ is the element of the NBO Fock matrix that couples the filled orbital σ to the unfilled σ^* and $\Delta\epsilon$ is the orbital energy splitting. There are usually only a few significant delocalizing interactions ($\Delta E^{(2)} > 1-2$ kcal mol^{-1}) per occupied NBO, since strong interaction typically requires both spatial proximity and the favorable orientation of the (σ,σ^*) pair. It is useful to relate the strength of interaction to orbital overlap. Since the NBOs form an orthogonal set of orbitals, we calculated the set of nonorthogonal pre-NBOs (PNBOs). This set is obtained by a procedure identical with that used for the NBOs, but neglecting the interatomic orthogonalization step. Second-order interaction energies are reported together with PNBO overlap. The interaction energies between metal hydrido fragments ($[MH_x^+]$) and hydrido anion (H^-) , dihydrogen molecule (H_2), and H_3^- fragments were further analyzed using the natural energy decomposition analysis (NEDA).[39] This is an energy partitioning procedure for molecular interactions based on the NBO approach[31−38] and implemented in GAMESS. The total interaction energy for the two fragments A and B was evaluated for self-consistent-field (SCF) wave functions by calculating electrostatic interaction (ES), charge transfer (CT), wave function deformation (DEF), and, in the

Table 2. Orbitals Used for the Active Space of the CASSCF Wave Functions

molecule	wave function	active space
H_2	CAS[2]	$1\sigma_g1\sigma_u$
H_3^-	CAS[3]	$1\sigma_g1\sigma_u1\sigma_g1\sigma_u1\sigma_g$
LiH	CAS[4]	$2\sigma3\sigma1\pi$
NaH	CAS[4]	$4\sigma5\sigma2\pi$
KH	CAS[4]	$6\sigma7\sigma3\pi$
CsH	CAS[4]	$3\sigma4\sigma2\pi$
ScH_3	CAS[7]	$2a_1'2e'3a_1'4a_1'3e'$
YH_3	CAS[7]	$2a_1'2e'3a_1'4a_1'3e'$
LaH_3	CAS[7]	$2a_1'2e'3a_1'4a_1'3e'$
TiH_4	CAS[10]	$2a_12f_23f_24f_2$
ZrH_4	CAS[9]	$2a_12f_23f_21e$
HfH_4	CAS[9]	$2a_12f_23f_21e$
C(Li)	CAS[6]	$2a_13a_14a_11b_12b_11b_2$
C(Na)	CAS[6]	$4a_15a_16a_12b_13b_12b_2$
C(K)	CAS[6]	$6a_17a_18a_13b_14b_13b_2$
C(Cs)	CAS[6]	$3a_14a_15a_12b_12b_23b_1$
C(Sc)	CAS[9]	4a′5a′2a″6a′7a′8a′3a″9a′10a′
C(Y)	CAS[9]	4a′5a′6a′2a″7a′8a′3a″9a′4a″
C(La)	CAS[9]	4a′5a′6a′2a″7a′3a″8a′9a′10a′
C(Ti)	CAS[11]	4a′5a′6a′2a″7a′8a′3a″9a′10a′11a′4a″
C(Zr)	CAS[11]	4a′5a′6a′2a"7a′8a′3a″9a′10a′4a″11a′
C(Hf)	CAS[11]	4a′5a′6a′2a″7a′8a′3a″9a′10a′4a″11a′
TS(Li)	CAS[6]	$2a_11b_13a_14a_12b_11b_2$
TS(Na)	CAS[6]	$4a_12b_15a_16a_13b_12b_2$
TS(K)	CAS[6]	$6a_13b_17a_18a_14b_13b_2$
TS(Cs)	CAS[6]	$3a_12b_14a_12b_23b_15a_1$
TS(Sc)	CAS[9]	$3a_14a_12b_22b_15a_13b_23b_16a_14b_1$
TS(Y)	CAS[9]	$3a_14a_12b_22b_15a_13b_23b_16a_11a_2$
TS(La)	CAS[9]	$3a_14a_12b_22b_15a_13b_23b_16a_11a_2$
TS(Ti)	CAS[11]	$3a_14a_12b_22b_15a_16a_13b_23b_17a_14b_21a_2$
TS(Zr)	CAS[11]	$3a_14a_12b_22b_15a_16a_13b_13b_21a_27a_18a_1$
TS(Hf)	CAS[11]	$3a_14a_15a_12b_22b_16a_13b_23b_11a_27a_18a_1$

(21) Lengsfield, B. H., III. *J. Chem. Phys.* **1980**, *73*, 382−390.
(22) Roos, B. O. In *Methods in Computational Molecular Physics*; Diercksen, G. H. F., Wilson, S., Eds.; D. Reidel: Dordrecht, The Netherlands, 1983; pp 161−187.
(23) Roos, B. O. In *Advances in Chemical Physics*; Lawley, K. P., Ed.; Wiley-Interscience: New York, 1987; Vol. 69, pp 339−445.
(24) Shepard, R. In *Advances in Chemical Physics*; Lawley, K. P., Ed.; Wiley-Interscience: New York, 1987; Vol. 69, pp 63−200.
(25) Schmidt, M. W.; Truong, P. N.; Gordon, M. S. *J. Am. Chem. Soc.* **1987**, *109*, 5217−5227.
(26) Ruedenberg, K.; Schmidt, M. W.; Dombek, M. M.; Elbert, S. T. *Chem. Phys.* **1982**, *71*, 41−49, 51−64, 65−78.
(27) Werner, H.-J. In *Advances in Chemical Physics*; Lawley, K. P., Ed.; Wiley-Interscience: New York, 1987; Vol. 69, pp 1−62.
(28) Møller, C.; Plesset, M. S. *Phys. Rev.* **1934**, *46*, 618.
(29) Shavitt, I. In *Methods of Electronic Structure Theory*; Schaefer, H. F., III, Ed.; Plenum Press: New York, 1977; Vol. 3, pp 189−276.
(30) Langhoff, S. R.; Davidson, E. R. *Int. J. Quantum Chem.* **1974**, *8*, 61.
(31) Foster, J. P.; Weinhold, F. *J. Am. Chem. Soc* **1980**, *102*, 7211.
(32) Carpenter, J. E.; Weinhold, F. *J. Mol. Struct.* **1988**, *169*, 41.
(33) Carpenter, J. E. Ph.D. Thesis, University of Wisconsin, Madison, WI, 1987.
(34) Reed, A. E.; Weinhold, F. *J. Chem. Phys.* **1983**, *78*, 4066.
(35) Reed, A. E.; Weinstock, R. B.; Weinhold, F. *J. Chem. Phys.* **1985**, *83*, 735.
(36) Weinhold, F.; Carpenter, J. E. *The Structure of Small Molecules and Ions*; Plenum: New York, 1988.
(37) Reed, A. E.; Curtiss, L. A.; Weinhold, F. *Chem. Rev.* **1988**, *88*, 899.
(38) Reed, A. E.; Weinhold, F. *J. Chem. Phys.* **1985**, *83*, 1736.
(39) Glendening, E. D.; Streitwieser, A. *J. Chem. Phys.* **1994**, *100*, 2900−2909.

Table 3. Optimized Geometrical Parameters (in Å) for the Hydrido Complexes MH_x and the Hydrogen/Hydrido Complexes C(M)

param	method	H_2	LiH	NaH	KH	CsH
M−H_L	SCF	0.7338	1.6406	1.9246	2.3712	2.6003
	CAS[2]	0.7545	1.6722	1.9558	2.4072	2.6528
	CAS[4]		1.6508	1.9232	2.3867	2.6528

param	method	**C**(Li)	**C**(Na)	**C**(K)	**C**(Cs)
M---H_2[a]	SCF	2.2832	2.8374	3.5403	4.4089
	CAS[4]	2.3255	2.9999	3.5252	4.4090
	CAS[6]	2.3086	3.0172	3.5373	4.5746
M−H_L	SCF	1.6357	1.9267	2.3759	2.6035
	CAS[4]	1.6665	1.9574	2.4096	2.6036
	CAS[6]	1.6446	1.9237	2.3877	2.6556
H−H	SCF	0.7362	0.7351	0.7345	0.7339
	CAS[4]	0.7567	0.7555	0.7548	0.7306
	CAS[6]	0.7567	0.7555	0.7550	0.7306

param[b]	ScH_3	YH_3	LaH_3	TiH_4	ZrH_4	HfH_4
M−H_L	1.8004	2.0141	2.1772	1.6497	1.8413	1.8350

param	**C**(Sc)	**C**(Y)	**C**(La)	**C**(Ti)	**C**(Zr)	**C**(Hf)
M---H_2[a]	2.8305	2.9165	3.3066	3.9935	3.9924	3.9926
M−H_L	1.8017[c]	2.0'16[c]	2.1633[c]	1.6500[c]	1.8406[c]	1.8344[c]
	1.8027[d]	2.017[d]	2.1640[d]	1.6501	1.8414	1.8350
				1.6509	1.8420	1.8357
H−H	0.7369	0.7373	0.7360	0.7341	0.7342	0.7343

[a] Distance from the metal atom to the center of mass of the H_2 fragment. [b] SCF values. [c] Bond length for the in-plane M−H bond. [d] Out-of-plane M−H bond lengths.

case of molecule fragments, geometry distortion (DIS) contributions (eq 2). For distances outside van der Waals contacts

$$\Delta E = \mathrm{CT} + \mathrm{ES} + \mathrm{DEF(A)} + \mathrm{DEF(B)} + [\mathrm{DIS(A)}] + [\mathrm{DIS(B)}] \quad (2)$$

the deformation terms describe the energy cost to polarize the fragment's charge distribution in the field of the other fragment. For smaller distances DEF is associated with the Pauli repulsions that prevent the fragment wave functions from significantly penetrating each other. Since the NEDA procedure evaluates all quantities in the complete basis set of the complex, the total interaction term ΔE corresponds to the counterpoise-corrected interaction energy of Boys and Bernardi.[40]

Results and Discussion

Equilibrium geometries and energies for the hydrogen molecule and the metal hydrides MH (M = Li, Na, K, Cs, ScH_2, YH_2, LaH_2, TiH_3, ZrH_3, HfH_3) are listed in Table 3. The calculated bond distances and angles are in good agreement with other theoretical data.

The first step in the activation reaction of dihydrogen is the formation of an adduct complex **C**(M) with the metal hydride; their general structures are shown in Figure 1.

Equilibrium geometries (Table 3) for the alkali-metal hydride/dihydrogen complexes have the general C_{2v} structure (**a** in Figure 1) in which the H_2 and MH fragment geometries closely resemble those of the separated reactants. Consequently, it is not surprising that these complexes are only weakly bound, by 1.91 (Li), 0.71 (Na), 0.32 (K), and 0.17 kcal mol^{-1} (Cs) at the full valence CI level (Table 5). Perturbative analysis of the fragment NBOs (Table 6) reveals only one significant CT interaction per complex, that between the

(40) Boys, S. F.; Bernardi, F. *Mol. Phys.* **1970**, *19*, 553.

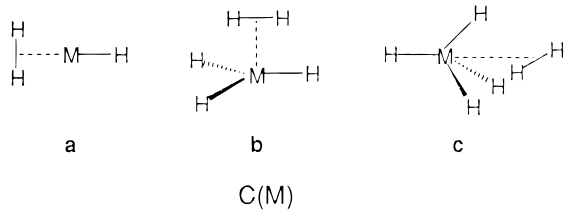

Figure 1. Structure types for coordination complexes of metal hydrides and H_2.

filled bond of H_2 (σ_{HH}) and the unfilled antibond (σ_{MH}*) on MH. The strength of this interaction weakens from −3.3 kcal mol^{-1} in **C**(Li) to −1.8 kcal mol^{-1} in **C**(Na), −0.6 kcal mol^{-1} in **C**(K), and −0.1 kcal mol^{-1} **C**(Cs), due to the diminished overlap of the H_2 bond with the increasingly diffuse antibonds of **C**(Na), **C**(K), and **C**(Cs). The weak nature of the CT interaction is also reflected in the natural charges (Table 6). The H_2 fragment has a small positive charge in each system (+0.011 (Li), +0.005 (Na), +0.001 (K), +0.0002 (Cs)), showing that there is but slight transfer of electron density from H_2 to MH in rough proportion to the strength of the $\sigma-\sigma$* interaction.

The equilibrium structures of the complexes of ScH_3, YH_3, and LaH_3 with H_2 (Table 3) differ somewhat from those of the **C**(M) alkali-metal complexes. Because of the steric restrictions of the MH bonds, the H_2 fragment cannot approach the group 3 metal centers from the backside of a MH bond. Instead, H_2 sits above the MH_3 fragment in a C_s symmetric arrangement that favors the CT interaction of the H_2 bond with a low-lying, extra-valence orbital of largely *d*-character on the metal centers. As in the alkali-metal complexes, this orbital interaction (Table 6) is relatively weak (−6.4 (Sc), −7.0 (Y), and −0.9 kcal mol^{-1} (La)) and the natural charge of H_2 (+0.012 (Sc), +0.012 (Y), and +0.005 (La)) reveals little transfer of electron density to MH_3 so that the **C**(M) complex is only weakly bound (by −1.58 (Sc), −1.93 (Y), and −3.29 kcal mol^{-1} (La) at the CISD+Q level). In the H_2 complexes of group 4 metal hydrides MH_4 (M = Ti, Zr, Hf) the bonds to dihydrogen are even weaker, since the repulsion of the ligand sphere is stronger (Table 5). The dihydrogen molecule sits above one face of the tetrahedron and shows only minor charge transfer into the empty σ^*_{M-H} orbital. Therefore, the natural charges of the hydrogen molecule in all of the group 4 metal complexes **C**(M) are less than 0.001 and the bond energies are less than 0.07 kcal mol^{-1}.

The hydrogen exchange transition-state structures have the general C_{2v} form shown as **TS**(M) (Table 7) for each of the metal centers investigated. For the

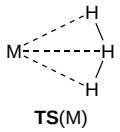

polyhydridic systems, M = MH_x^+ in the transition states with the reflection plane containing the H_3 unit, shown above, bisecting the MH_x angle (x = 2 for M = Sc, Y, and La; x = 3 for M = Ti, Zr, and Hf). These structures are of high energy relative to the separated reactants MH and H_2 (E(**TS**) = 16.69 (Li), 21.68 (Na), 15.74 (K), 13.47 (Cs), 10.28 (Sc), 9.54 (Y), 8.14 (La), 31.53 (Ti), 45.88 (Zr), and 40.50 kcal mol^{-1} (Hf)). Although these

Table 4. Total Energies (au) for the Hydrides MH_x

method	H_2	LiH	NaH	KH	CsH
SCF	−1.131 434	−7.981 811	−162.377 721	−599.666 800	−20.390 479
CAS[2]	−1.149 747	−7.998 510	−162.397 328	−599.686 532	−20.408 040
CAS[4]		−8.002 536	−162.401 730	−599.689 491	−20.408 040
MP2[d]	−1.158 180	−7.999 812	−162.398 037	−599.684 773	−20.407 764
CI[d,e]	−1.165 832	−8.006 546	−162.406 124	−599.691 986	−20.413 790

method	ScH_3[a]	YH_3[a]	LaH_3[a]	TiH_4[b]	ZrH_4[b]	HfH_4[b]
SCF	−47.670 582	−39.193 075	−32.484 048	−59.669 994	−48.279 891	−50.627 051
CAS[n+1][c,d]	−47.697 049	−39.235 769	−32.529 625	−59.766 842	−48.353 408	−50.688 629
MP2[d]	−47.719 922	−39.251 915	−32.541 861	−59.806 438	−48.375 781	−50.717 406
CI[d,e]	−47.740 433	−39.269 869	−32.559 648	−59.839 342	−48.404 009	−50.743 466

[a] D_{3h} symmetry. [b] T_d symmetry. [c] For M = Sc, Y, and La, n = 6; for M = Ti, n = 9; for M = Zr and Hf, n = 8. The higher value for Ti is required because the highest level used in the CI is degenerate for this case. Such degeneration did not occur in the complex. [d] Calculated at the SCF optimized geometry. [e] Full valence CI for H_2 and the alkali-metal hydrides; single and double CI with Davidson's correction[30] for MH_x.

Table 5. Energies[a] for the Hydrogen/Hydrido Complexes C(M)

method	**C**(Li)	**C**(Na)	**C**(K)	**C**(Cs)
SCF	−9.115 777 4 (−1.59)	−163.510 093 3 (−0.59)	−600.798 699 0 (−0.29)	−21.522 141 5 (−0.14)
CAS[4]	−9.150 245 2 (−1.25)	−163.547 547 5 (−0.30)	−600.836 466 4 (−0.12)	−21.530 305 4 (−0.06)
CAS[6]	−9.154 427 9 (−1.35)	−163.552 025 9 (−0.34)	−600.839 492 5 (−0.16)	−21.547 946 7 (−0.08)
MP2[c]	−9.161 416 6 (−2.15)	−163.557 683 5 (−0.92)	−600.843 495 3 (−0.34)	−21.566 000 7 (−0.04)
CISD+Q[c,d]	−9.176 335 1 (−2.48)	−163.574 227 0 (−1.43)	−600.859 361 9 (−0.97)	
CI[c,e]	−9.175 428 3 (−1.91)	−163.573 085 2 (−0.71)	−600.858 320 2 (−0.32)	−21.579 568 3 (−0.17)

method	**C**(Sc)	**C**(Y)	**C**(La)	**C**(Ti)	**C**(Zr)	**C**(Hf)
SCF	−48.785 727 (−1.13)	−40.326 922 (−1.51)	−33.619 447 (−2.50)	−60.801 753 (−0.20)	−49.411 591 (−0.17)	−51.758 779 (−0.19)
CAS[n+1][b,c]		−40.374 212 (+7.09)	−33.685 656 (−3.95)	−60.925 410 (−5.54)	−49.493 588 (−6.01)	−51.829 122 (−2.03)
MP2[c]	−48.881 040 (−1.85)	−40.413 429 (−2.09)	−33.705 206 (−3.24)	−60.965 281 (−0.41)	−49.534 620 (−0.41)	−51.876 260 (−0.43)
CISD+Q[c,d]	−48.909 336 (−1.58)	−40.439 330 (−1.93)	−33.731 268 (−3.29)	−61.005 035 (−0.09)	−49.570 318 (−0.04)	−51.909 954 (−0.07)

[a] Absolute energies in au; relative energies (in parentheses) with respect to the separated adducts (Table 4) are given in kcal mol^{-1}. [b] For M = Sc, Y, and La, n = 8; for M = Ti, Zr, and Hf, n = 10. Compare Table 4, note *c*. [c] Calculated at the SCF optimized geometry. [d] Single and double excitation CI with Davidson's correction.[30] [e] Full valence CI.

Table 6. NBO Analysis of the Significant CT Interactions in the Complexes C(M) and Results of the Natural Energy Decomposition Analysis (kcal mol^{-1}) using the SCF Wave Function

	interaction	$\Delta E^{(2)}$ [a]	q(SCF)[b]	q(CI)[b]	ΔE[c]	CT	ES	DEF(D)[d]	DEF(A)[e]
C(Li)	$\sigma_{HH}-\sigma_{LiH}$*	−3.3	0.010	0.011	−1.2	−6.2	−1.5	4.1	2.4
C(Na)	$\sigma_{HH}-\sigma_{NaH}$*	−1.8	0.004	0.005	−0.5	−2.0	−1.1	2.0	0.6
C(K)	$\sigma_{HH}-\sigma_{KH}$*	−0.6	0.001	0.001	−0.2	−0.7	−0.5	0.5	0.4
C(Cs)	$\sigma_{HH}-\sigma_{CsH}$*	−0.1	<0.001	0.006	−0.1	−0.2	−0.1	0.1	0.2
C(Sc)	$\sigma_{HH}-3d_{z^2}$	−6.4	0.012	0.015	−1.1	−6.2	−3.4	6.4	1.9
C(Y)	$\sigma_{HH}-4d_{z^2}$	−7.0	0.012	0.014	−1.3	−6.8	−1.8	5.1	2.2
C(La)	$\sigma_{HH}-5d_{z^2}$	−0.9	0.005	0.008	−1.0	−2.3	−1.5	1.9	1.0
C(Ti)	$\sigma_{HH}-3d_{z^2}$	−0.1	<0.001	0.001	−0.1	−0.4	−0.8	0.7	0.4
C(Zr)	$\sigma_{HH}-4d_{z^2}$	−0.3	<0.001	0.001	−0.1	−0.7	−0.9	1.0	0.6
C(Hf)	$\sigma_{HH}-5d_{z^2}$	−0.45	<0.001	0.001	−0.2	−0.8	−0.9	1.0	0.5

[a] Second-order interaction energies in kcal mol^{-1}. [b] Natural charge of the H_2 fragment. [e] For dissociation into H_3^-. [d] D = donor. [e] A = acceptor.

energies (Table 8) depend somewhat on the level of theory (e.g., the energy of **TS**(Sc) varies from 10.28 kcal mol^{-1} at CISD+Q to 16.07 kcal mol^{-1} at CAS[9]), each level suggests that the barrier to exchange is lowest for lanthanum and highest for the group 4 metals. Similar results for some of these systems have been found previously. Kaufmann and Schleyer[8] reported energies for **TS**(Li) and **TS**(Na) of 15.7 and 19.8 kcal mol^{-1} at MP2/6−31++G(d,p). With the GVB method and a double-ζ basis set, Steigerwald and Goddard[41] calculated a barrier for exchange on the $ScHCl_2 + H_2$ surface of 17.4 kcal mol^{-1}.

(41) Steigerwald, M. L.; Goddard, W. A., III. *J. Am. Chem. Soc.* **1984**, *106*, 308.
(42) Huzinaga, S. *J. Chem. Phys.* **1965**, *42*, 1293.
(43) Dunning, T. H. *J. Chem. Phys.* **1970**, *53*, 2823.
(44) Dunning, T. H. *J. Chem. Phys.* **1971**, *55*, 716−723.
(45) McLean, A. D.; Chandler, G. S. *J. Chem. Phys.* **1980**, *72*, 5639−5648.
(46) Wachters, A. J. H. *J. Chem. Phys.* **1970**, *52*, 1033−1036.

Table 7. Optimized Geometrical Parameters[a] for the Hydrogen Exchange Transition States TS(M)

(a) M = Li, Na, K, Cs

param	method	**TS**(Li)	**TS**(Na)	**TS**(K)	**TS**(Cs)
$M-H_c$[b]	SCF	1.6174	1.9615	2.3910	2.6157
	CAS[4]	1.6149	1.9545	2.3832	2.6157
	CAS[6]	1.6190	1.9603	2.3947	2.6251
$M-H_t$[c]	SCF	1.7570	2.1157	2.5105	2.7034
	CAS[4]	1.7673	2.1206	2.5184	2.7034
	CAS[6]	1.7678	2.1225	2.5205	2.7167
H_c-H_t	SCF	1.0555	1.0604	1.0561	1.0455
	CAS[4]	1.0848	1.0909	1.0827	1.0455
	CAS[6]	1.0575	1.0622	1.0549	1.0509
$\angle H_t-H_c-H_t$	SCF	158.36	166.30	167.97	166.84
	CAS[4]	158.24	166.18	168.67	166.84
	CAS[6]	159.32	167.15	168.77	167.21

(b) M = Sc, Y, La, Ti, Zr, Hf[d]

param	**TS**(Sc)	**TS**(Y)	**TS**(La)	**TS**(Ti)	**TS**(Zr)	**TS**(Hf)
$M-H_c$[b]	1.9252	2.1174	2.3046	1.8710	2.0548	1.9609
$M-H_t$[c]	1.9268	2.1467	2.3172	1.8827	2.0471	1.9449
$M-H_L$[e]	1.7990	2.0175	2.1670	1.6762	1.8524	1.8614
				1.6103	1.8139	1.8900
H_c-H_t	1.0203	1.0309	1.0280	1.0242	1.0260	1.0088
$\angle H_t-H_c-H_t$	150.62	155.19	155.65	149.59	150.19	148.31
$\angle H_t-M-H_t$	61.27	55.94	51.40	63.33	57.70	59.87

[a] Internuclear distances in Å and angles in deg. [b] Distance from the metal center to the central hydrogen atom of the H_3 fragment. [c] Distance from the metal center to the terminal hydrogen atoms of the H_3 fragment. [d] SCF optimized geometries. [e] Distance from the metal center to the other hydrogen atoms of the ligand sphere.

Table 8. Total Energies[a] for the Hydrogen Exchange Transition States TS(M)

method	**TS**(H_3^-)	**TS**(Li)	**TS**(Na)	**TS**(K)	**TS**(Cs)
SCF	−1.593 084	−9.077 969	−163.468 382	−600.767 285	−21.496 719
	(15.95)	(22.14)	(25.59)	(19.42)	(15.81)
CAS[4]	−1.599 790[e]	−9.100 881	−163.491 569	−600.790 020	−21.496 720
	(37.63)	(29.73)	(34.83)	(29.03)	(25.98)
CAS[6]		−9.120 494	−163.510 838	−600.809 301	−21.537 325
		(19.95)	(25.50)	(18.79)	(16.35)
MP2[c]	−1.645 080	−9.131 500	−163.522 731	−600.818 960	−21.545 722
	(10.77)	(16.62)	(21.01)	(15.06)	(12.69)
CISD+Q[c,d]		−9.146 386	−163.538 037	−600.833 322	
		(16.31)	(21.28)	(15.37)	
CI[c,f]	−1.660 462	−9.145 785	−163.537 401	−600.832 728	−21.558 156
	(4.40)	(16.69)	(21.68)	(15.74)	(13.47)

method	**TS**(Sc)	**TS**(Y)	**TS**(La)	**TS**(Ti)	**TS**(Zr)	**TS**(Hf)
SCF	−48.755 384	−40.298 104	−33.592 829	−60.738 005	−49.322 288	−51.676 996
	(17.91)	(16.57)	(14.21)	(39.80)	(55.87)	(51.13)
CAS[n+1][b,c]	−48.821 181	−40.359 549	−33.657 119	−60.847 228	−49.413 021	−51.757 613
	(16.07)	(16.29)	(13.96)	(43.52)	(56.56)	(50.68)
MP2[c]	−48.861 855	−40.394 470	−33.687 150	−60.911 984	−49.461 150	−51.811 548
	(10.19)	(9.81)	(8.09)	(33.03)	(45.69)	(40.18)
CISD+Q[c,d]	−48.890 432	−40.421 044	−33.713 050	−60.955 464	−49.497 263	−51.845 306
	(10.28)	(9.54)	(8.14)	(31.53)	(45.88)	(40.50)

[a] Absolute energies in au; relative energies (in parentheses) with respect to the separated educts (Table 4) are given in kcal mol^{-1}. [b] For M = Sc, Y, and La, n = 8; for M = Ti, Zr, and Hf, n = 10. [c] Calculated at the SCF optimized geometry. [d] Single and double excitation CI with Davidson's correction.[30] [e] CAS[5] values. [f] Full valence CI.

Unlike the structures **C**(M) that arise from the weak association of MH and H_2, the **TS**(M) structures are best described as strongly interacting complexes of the metal cations M^+ with the H_3^- anion. The anionic character of the latter is clearly reflected in the natural charges (CI) of the H_3 fragment (−0.890 (Li), −0.930 (Na), −0.985 (K), −0.946 (Cs), −0.596 (Sc), −0.647 (Y), −0.811 (La), −0.420 (Ti), −0.480 (Zr), −0.373 (Hf); cf. Table 9). These charges indicate that the association for the alkali metals and lanthanum is largely ionic. For the other metals the charges suggest that CT interactions contribute importantly by transferring a significant amount of electron density from the H_3^- fragment to the metal center. For the transition-metal **TS**'s about 0.35−0.59 electron is transferred from H_3^- to MH_x^+.

Perturbative analysis (Table 9) of the fragment NBOs again provides insight into the interactions that are responsible for CT. The H_3^- fragment has four electrons occupying two three-center bonds: an in-phase bonding combination (σ_b) of the three hydrogen 1s orbitals and an out-of-phase nonbonding combination (σ_{nb}) involving only the 1s orbitals of the terminal hydrogens. The interactions of these two donor orbitals with acceptor orbitals on the metal are what lead to CT. In the case of transition-metal **TS**(M)s, there are two dominant

(47) Ross, R. B.; Powers, J. M.; Atashroo, T.; Ermler, W. C.; Lajohn, L. A.; Christiansen, P. A. *J. Chem. Phys.* **1990**, *93*, 6654−6670.
(48) Clark, T.; Chandrasekhar, J.; Spitznagel, G. W.; Schleyer, P. v. R. *J. Comput. Chem.* **1983**, *4*, 294.
(49) Hariharan, P. C.; Pople, J. A. *Theor. Chim. Acta* **1973**, *28*, 213−222.

Table 9. NBO Analysis of the Significant CT Interactions of the Transition States TS(M)

	interaction[a]	$\Delta E^{(2)}$ [b]	S[c]	q(SCF)[d]	q(CI)[d]
TS(Li)	$\sigma_{nb}-3p_\pi$	−16.0	0.534	−0.910	−0.890
	σ_b-2s	−10.1	0.704		
TS(Na)	$\sigma_{nb}-3p_\pi$	−5.8	0.531	−0.948	−0.930
	σ_b-3s	−5.2	0.600		
TS(K)	$\sigma_{nb}-3d_\pi$	−1.6	0.476	−0.988	−0.985
	σ_b-4s	−1.3	0.424		
TS(Cs)	$\sigma_{nb}-5d_\pi$	−2.7	0.597	−0.944	−0.946
	σ_b-5d_σ	−7.2	0.432		
TS(Sc)	$\sigma_{nb}-3d_\pi$	−144.0	0.645	−0.591	−0.596
	σ_b-3d_σ	−71.5	0.517		
TS(Y)	$\sigma_{nb}-4d_\pi$	−107.3	0.617	−0.676	−0.647
	σ_b-4d_σ	−57.6	0.575		
TS(La)	$\sigma_{nb}-5d_\pi$	−36.8	0.580	−0.835	−0.811
	σ_b-5d_σ	−24.2	0.591		
TS(Ti)	$\sigma_{nb}-3d_\pi$	−212.4	0.578	−0.481	−0.420
	σ_b-3d_σ	−93.3	0.655		
TS(Zr)	$\sigma_{nb}-4d_\pi$	−199.7	0.581	−0.512	−0.480
	σ_b-4d_σ	−72.3	0.702		
TS(Hf)	$\sigma_{nb}-5d_\pi$	−270.4	0.610	−0.408	−0.373
	σ_b-5d_σ	−106.1	0.746		

[a] Donor−acceptor interactions listed. In each case, the donor is either the bonding (σ_b) or nonbonding (σ_{nb}) orbital of H_3^- and the acceptor is an unfilled orbital on M^+. [b] Second-order interaction energy, in kcal mol^{-1}. [c] Orbital overlap. [d] Natural charge of the H_3^- fragment.

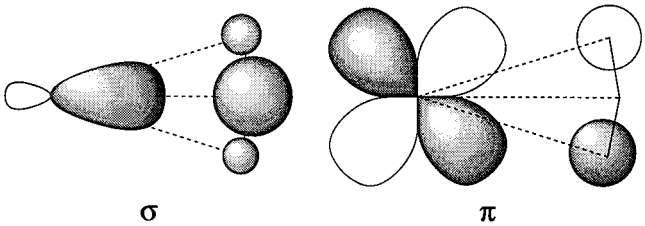

Figure 2. Interaction between the bonding orbital (σ_b) of the H_3^- fragment and the d_σ orbital of a transition metal and between the nonbonding orbital (σ_{nb}) and the d_π orbital.

interactions (Figure 2), a π-type interaction between σ_{nb} and the d_π orbital of MH_x^+ (144.0 (Sc)−270.4 (Hf) kcal mol^{-1} (Hf)) and a σ-type interaction between σ_b and an extra-valence orbital of primarily d_σ character (71.5 (Sc)−106.1 kcal mol^{-1} (Hf)). Steigerwald and Goddard[41] also noted the importance of d orbitals in the transition state of $ScHCl_2 + H_2$. They calculated two three-center bonds that closely resemble the orbitals of Figure 2. Clearly, d orbital participation strongly stabilizes the transition-metal transition states.

The NEDA analysis of the interactions of metal groups with H_3^- is summarized in Tables 10. This analysis also shows that CT is much less for the alkali metals than for the other systems. Many of the derived energy values are large, confirming the strong interactions of the transition metals with the H_3^- fragment; the results also demonstrate that the NEDA procedure is generally more valuable for analyzing weak interactions.[39]

Charge transfer plays only a small role in the alkali-metal **TS**(M) wave functions, much smaller than in the transition-metal **TS**(M). The CASSCF wave functions provide a further indication of the role of the acceptor function on the metal that has π symmetry. Whereas the more extended wave functions (CAS[6] for the alkali metals, CAS[9]−CAS[11] for the transition metals) predict transition-state energies that are similar to the MP2 and CI values, the smaller wave functions (CAS-[4] and CAS[8]) have energies that are too high by about 10 kcal mol^{-1}. Since the latter do not include the metal acceptor function in the active space, the correlation of σ_{nb} is largely neglected and the transition-state energy is raised relative to reactants. Although an accurate description of metal-containing compounds often requires multireference methods, in each of the present cases the CI coefficient of the leading configuration of the CAS expansion is greater than 0.98, suggesting that single-reference methods (SCF, MP2, CISD) are adequate.

One of the particularly interesting observations of this study is the enormous disparity of CT stabilization in the potassium and scandium transition states. Although the strongest orbital interaction in each involves σ_{nb} and d_π on the metal, CT is strongly favored in the scandium case (144.0 vs 1.6 kcal mol^{-1}). We checked that this result is not due to any deficiency in the potassium d orbital basis compared to that of scandium, since the former is described by a single uncontracted Gaussian, whereas the latter is a double-ζ contraction of five Gaussians. To investigate this situation further, the potassium d basis function was replaced by the two scandium functions, each scaled by 0.75 (this scale factor was chosen to minimize the SCF energy of KH). Extending the potassium basis set in this fashion had little effect on either the qualitative features of the hydrogen exchange potential surface or the CT perturbative analysis. The transition state was stabilized somewhat, from 19.42 to 18.73 kcal mol^{-1} (at the SCF level), and the leading orbital interaction was strengthened from -1.6 to −4.7 kcal mol^{-1}. Clearly, the disparate role of CT in the scandium and potassium systems cannot be attributed to an inadequate potassium basis.

Next, we focus attention on the energies of the transition-state structures. The present analysis suggests that the relative stabilities of these structures are associated with the extents of charge transfer (Figure 3), which in turn depend on the availability of low-lying acceptor orbitals on the metal in close proximity and of proper symmetry to interact with the orbitals of the donor fragment. Strong charge transfer (Figure 4, positive differences) stabilizes the transition state, thereby enhancing the rate of hydrogen exchange. Exchange is particularly favorable at group 3 metals, in which the transition state is strongly stabilized by interactions with the vacant d orbitals. Potassium, on the other hand, appears to be an exception. Compared to the other systems examined here, the potassium transition state is only weakly stabilized by charge transfer, and yet the energy of this structure lies intermediate between that of scandium and lithium. Although stabilization of the transition states by low-lying vacant d orbitals can explain the differences in activation barrier between the lighter alkali metals and group 3 transition metals, cesium and the group 4 metals reveal that alternative factors are also important. Using the activation energy of the model reaction of a "free" hydride anion with a H_2 molecule (15.95 kcal mol^{-1}) as a standard to evaluate the performance of several metal−hydride systems shows that within the groups of alkali and group 3 metals the heaviest member has the lowest barrier for exchange (Figure 3). In seeking reasons for this behavior, one important factor for the propagation of the exchange reaction is the ability of the central atom to first coordinate a

Table 10. Natural Energy Decomposition Analysis Using the SCF Wave Function

(a) Total Interaction Energy (kcal mol^{-1})

	ΔE	CT	ES	DEF(D)[a]	DEF(A)[b]	DIS(D)[a]	DIS(A)[b]
LiH	−162.3	−31.7	−179.7	36.8	12.2		
TS(Li)	−156.1	−21.2	−179.6	27.1	15.2	2.4	
NaH	−142.3	−26.8	−173.4	42.5	15.4		
TS(Na)	−132.7	−12.7	−158.2	22.6	14.6	1.0	
KH	−115.0	−11.9	−155.4	35.0	17.3		
TS(K)	−111.7	−3.4	−143.0	19.7	14.3	0.8	
CsH	−107.2	−19.0	−138.4	29.0	21.2		
TS(Cs)	−107.6	−12.8	−133.8	18.1	20.1	0.8	
ScH_3	−204.8	−136.5	−276.2	150.2	54.4		3.4
TS(H_2ScH_3)	−203.0	−133.4	−263.1	124.0	62.0	4.8	2.8
YH_3	−195.4	−93.1	−262.3	111.9	44.8		3.4
TS(H_2YH_3)	−194.8	−97.1	−235.1	81.0	50.5	3.4	2.4
LaH_3	−176.3	−64.9	−245.8	87.0	43.2		4.2
TS(H_2LaH_3)	−178.1	−50.9	−229.0	48.2	47.4	3.2	3.0
TiH_4	−221.3	−244.8	−258.4	198.5	77.5		5.9
TS(H_3TiH_3)	−197.5	−166.6	−335.7	223.0	70.2	5.0	6.5
ZrH_4	−222.7	−176.1	−285.3	175.3	60.7		2.7
TS(H_3ZrH_3)	−182.8	−150.7	−263.7	131.2	69.9	4.9	25.6
HfH_4	−230.2	−166.9	−301.9	176.9	59.0		2.7
TS(H_3HfH_3)	−195.1	−195.2	−252.9	142.4	87.7	5.9	17.0

(b) Interaction Energy Differences (kcal mol^{-1}) between Ground and Transition State Fragments[c,d]

	$\Delta\Delta E$	ΔCT	ΔES	ΔDEF(D)[a]	ΔDEF(A)[b]	ΔDIS(D)[a]	ΔDIS(A)[b]
Li	6.2	10.5	0.1	−9.8	3.0	2.4	0
Na	9.6	14.2	15.3	−20.0	−0.8	1.0	0
K	3.4	8.5	12.4	−15.2	−3.0	0.8	0
Cs	−0.3	6.3	4.6	−10.9	−1.1	0.8	0
Sc	1.9	3.2	13.1	−26.2	7.6	4.8	−0.6
Y	0.6	−3.9	27.1	−30.9	5.7	3.4	−1.0
La	−1.8	14.0	16.7	−38.8	4.2	3.2	−1.2
Ti	23.8	78.2	−77.3	24.5	−7.3	5.0	0.6
Zr	39.8	25.3	21.6	−44.0	9.2	4.9	22.8
Hf	35.1	−28.4	48.9	−34.5	28.7	5.9	14.4

[a] Donor. [b] Acceptor. [c] Ground state fragments are $[H_{n-1}M]^+$ and H^- (Li−Cs, $n = 1$; Sc−La, $n = 2$; Ti−Hf, $n = 3$). [d] Transition-state fragments are $[H_{n-1}M]^+$ and H_3^-.

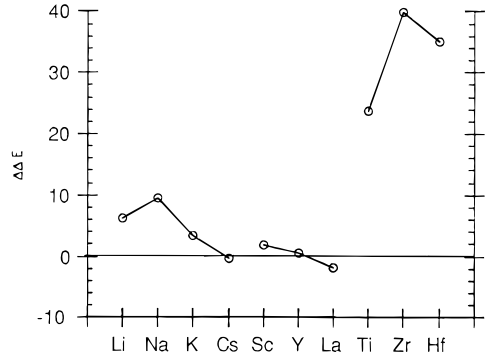

Figure 3. Total activation energy differences (kcal mol^{-1}) relative to the $H^- + H_2$ reaction barrier.

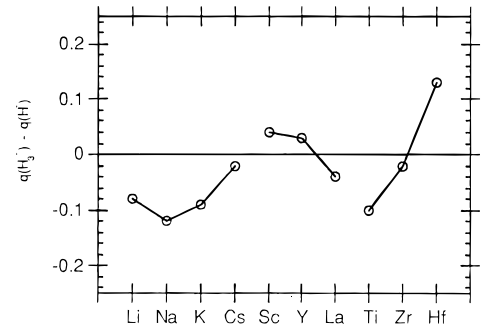

Figure 4. Differences in partial charges between the TS (H_3^-) and hydrido ligand fragments.

hydrogen molecule at a vacant position to allow a σ_{HH} donor−p*(d*) acceptor interaction. However, as the exchange reactions proceed, a second interaction becomes more important: donation of electron density into the empty antibonding σ^*_{HH} orbital. The latter interaction can be considered as the key interaction to lengthen the H−H bond, leading to the transition-state structure. The hydrido ligand involved in this interaction needs enough electron density to donate some into the antibonding σ^*_{HH} of the approaching hydrogen molecule. Therefore, it is not surprising that the hydrides of cesium and lanthanum, the heaviest metals within their group, have hydrido ligands that carry more negative charge than the ligands of their lighter analogs and show the lowest barriers for exchange. The longer metal−hydrido bonds lead to decreasing charge transfer, less polarization, and deformation of the wave functions and favor the ability of the hydrido ligand to weaken the H−H bond of an approaching hydrogen molecule. That is, these highly ionic hydrides more closely approximate the standard reaction of hydride anions.

The stabilization of the transition state by empty d orbitals as well as the strength of the M−H bond in the metal hydrides both help to rationalize the trends in the exchange reactions with the alkali and group 3 metals. However, for the group 4 metals a third factor also seems to be important. Zirconium and hafnium hydrides have high barriers for the exchange reaction (39.83 and 35.08 kcal mol^{-1} above the activation barrier for the model reaction, Table 10b). Hafnium has this high barrier, although it is the only transition metal in which more charge is transferred by the H_3^- ligand in the transition state than by the hydrido ligand in the starting complex. Two main interactions oppose the

gain in energy by the increased charge transfer. In a direct response to the transfer of 0.59 electron from the H_3^- ligand (0.13 more than the H^- ligand is able to donate in HfH_4) the electrostatic interaction is strongly reduced. Furthermore, and as is true for zirconium as well, the transition-state geometry with six ligands increases the strain within the molecule, as can be analyzed in terms of the acceptor fragment deformation $\Delta DIS([MH_x]^+)$ (Table 10b). Both effects together with the low partial charges at the hydrido ligands are responsible for the high activation barriers for group 4 transition-metal exchanges. Moreover, the trend in activation barriers as one goes from titanium hydride to hafnium hydride is different from that in groups 1 and 3. The reason for the reversed trend is mainly due to the enormous change (+0.23 Å) in bond distances between titanium hydride and the corresponding transition-state structure. This bond difference is large compared to group 3 metals, and therefore the amount of charge transferred in the transition state is much smaller. Although an increase in electrostatic interaction between the H_3^- fragment and the metal core fragment is able to compensate for the loss in charge transfer stabilization, the wave function of the H_3^- fragment as well as its geometry are strongly deformed.

Conclusion

For the alkali metals, the TS energy depends primarily on the electrostatic interaction of H_3^- with M^+ in the TS compared to that for H^- and M^+ in the reactants. This difference is not monotonic with cation size. A comparison of the distance changes between metal cation and hydride in MH and the distances to the terminal hydrogens (those that carry the bulk of the negative charge) in H_3^- is instructive. This distance difference increases from 0.12 Å for Li to 0.20 Å for Na but decreases again to 0.14 Å for K and 0.10 Å for Cs. The distance changes for group 3 metals varies relatively within the same region, 0.10−0.12 Å, whereas the variations are greater for the group 4 metals (0.23 (Ti), 0.20 (Zr), and 0.10 Å (Hf)). The small change for hafnium results from the completely filled 4f shell (lanthanide contraction).

For group 3 metals, the relatively low TS barrier is also explicable largely on electrostatic terms, but these TS's are clearly stabilized still further by covalent bonding involving charge transfer from the H_3^- fragment to an empty d orbital on the metal. Unfortunately, a strong involvement of an empty d orbital system not only lowers the energy of the transition state but also stabilizes the metal hydrido bond of the starting complex itself, leading to a reduced negative charge at the hydrido ligand and a less polarized bond. As a result, the ability of this ligand in donating electron density into the empty σ^* orbital of the approaching hydrogen molecule is strongly reduced. This situation is found for the group 4 metals, in which the amount of charge transfer interaction reaches the level of electrostatic interaction, leading to a higher activation barrier for exchange. These results might well be generalized to other transition metals.

Acknowledgment. This research was supported in part by NSF Grants Nos. CHE 8721134 and 9221277 and was partly done at the College of Chemistry Graphics Facility, which is supported by NIH Grant No. 850RR05651A. A.H.N. acknowledges grants by the Miller Institute for Basic Research in Science, Berkeley, CA, and the Alexander von Humboldt-Foundation, Bonn-Bad Godesberg, FRG. We also thank Michael Eckhart for some preliminary calculations.

OM960350N